

Ano-SuPs: Multi-size anomaly detection for manufactured products by identifying suspected patches

Hao Xu ^a Juan Du ^{a,b} and Andi Wang ^c

^a Smart Manufacturing Thrust, The Hong Kong University of Science and Technology (Guangzhou), Guangzhou, China.

^b Department of Mechanical and Aerospace Engineering, The Hong Kong University of Science and Technology, Hong Kong SAR, China.

^c The Polytechnic School, Arizona State University, Mesa, AZ, USA.

Abstract

Image-based systems have gained popularity owing to their capacity to provide rich manufacturing status information, low implementation costs and high acquisition rates. However, the complexity of the image background and various anomaly patterns pose new challenges to existing matrix decomposition methods, which are inadequate for modeling requirements. Moreover, the uncertainty of the anomaly can cause anomaly contamination problems, making the designed model and method highly susceptible to external disturbances. To address these challenges, we propose a two-stage strategy anomaly detection method that detects anomalies by identifying suspected patches (Ano-SuPs). Specifically, we propose to detect the patches with anomalies by reconstructing the input image twice: the first step is to obtain a set of normal patches by removing those suspected patches, and the second step is to use those normal patches to refine the identification of the patches with anomalies. To demonstrate its effectiveness, we evaluate the proposed method systematically through simulation experiments and case studies. We further identified the key parameters and designed steps that impact the model's performance and efficiency.

Keywords: Anomaly detection; Vision transformer; Multi-size anomaly; Quality inspection.

1 Introduction

In manufacturing systems, image data frequently provides detailed information about manufacturing status, such as temperature distribution and surface quality Fang et al. (2019). As the image data collection in the production environment becomes more accessible and less expensive (Shi (2023)), various manufacturing processes have employed image-based

sensing and real-time decision systems for anomaly detection, for quickly inferring the product quality based on the collected image data. With these images, the faults that occur in the manufacturing processes can be timely identified to avoid products with unacceptable quality (Du et al. (2021)).

In this paper, we consider the above image-based defect and anomaly identification problem in the context of manufacturing and production systems. Specifically, we consider the common yet challenging scenario where the anomalies may only appear in certain regions of each image. The specific assumptions on the non-anomaly regions and anomalies are as follows:

- Even the non-defective regions of the image samples have a certain degree of variations, given the randomness of the disturbance of the data acquisition environment (e.g., lighting and angle) and the stochastic nature of the manufacturing processes.
- On the abnormal images, there can be either one or multiple abnormal regions (defects). Besides, these abnormal regions may have different sizes, even within the same image.

The following example illustrates the anomaly detection scenario considered in this paper. Three images of metal grid products from the MVTec dataset (Bergmann et al. (2019)) are displayed in Figure 1. Among them, Figure 1 (a) shows the image data collected for the normal product, where the surface morphology exhibits a sophisticated geometric pattern, while Figure 1 (b) and (c) shows the image data with anomalies. While these three images have common patterns of metal meshes and the latter two have significant defects, there is a certain level of flexibility in the background of these images, due to the orientation of the metal grid as well as the brightness distribution. As for the anomalies, Figure 1 (b) and (c) display different defective patterns: there are multiple defects in the linkage of the metal grid within Figure 1 (b) while Figure 1 (c) shows a metal grid with a tangled thread caused by process fault. Anomalies from the two latter figures have distinct forms that both lead to non-compliance with the quality standards and the size and the locations of the anomalies are also different.

Local defect identification problems like the one introduced above are pervasive in the manufacturing industry from semiconductor manufacturing (Wang and Tsung (2005)) to

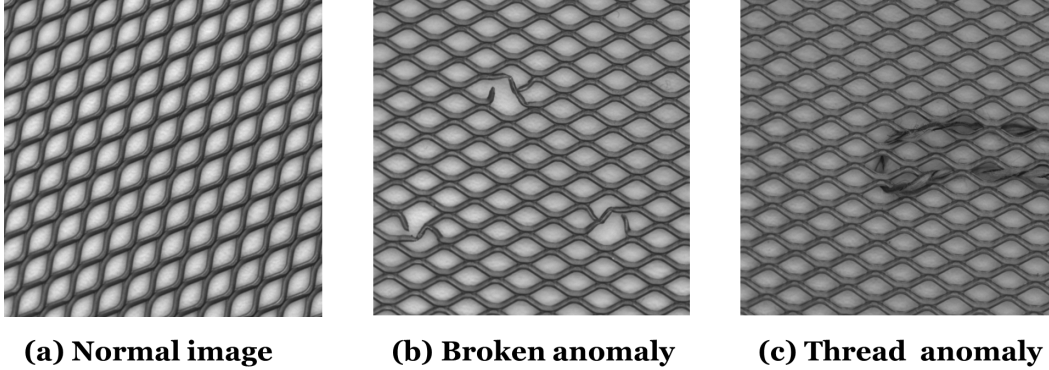


Figure 1: A complex representation product with different patterns of anomaly from MVTEC dataset (a) Normal image with complex backgrounds. (b) Broken anomaly. (c) Thread anomaly.

textile production (Behera (2004)) to steel rolling (Yan et al. (2018)). However, anomaly detection based on images obtained from the production systems is a difficult task, given both the variability of the normal regions and the number and sizes of multiple defective regions.

Among existing image monitoring approaches, the reconstructive deep learning approach is the most appropriate for our scenario. As will be introduced in the literature review, the existing image monitoring approaches can be generally divided into two classes of approaches: additive matrix decomposition approach and deep learning approach. Additive matrix decomposition approaches typically require stringent requirements that the background is a smooth or low-rank (Yan et al. (2017), Mou et al. (2023)) image. In manufacturing practice, however, these assumptions seldom hold and thus the matrix decomposition approach is less effective than the deep learning approach. With the deep-learning approach, image-based anomaly detection can either be based on the latent representation of the image or the reconstruction error of the image. The general idea of the reconstructive method is to first develop a reconstructive model that generates an individual patch of an image based on a few other patches. Then the similarity between a patch and its reconstruction from other patches can be used to identify anomalies. Compared with monitoring the latent representations, the reconstructive approach is more robust and intuitive.

However, existing reconstructive deep learning methods have a common cause that af-

fects the accuracy of anomaly detection: when reconstructing a *normal* patch in an image using other patches that contain anomalies, the reconstruction is influenced by these abnormal inputs, thereby yielding an *abnormal* patch and resulting in imprecise anomaly detection. We refer to this issue as the *anomaly contamination problem*. To illustrate this, Figure 2 shows two reconstruction cases of SSIM-AE (Bergmann et al. (2022)), a classical deep learning unsupervised anomaly detection method, affected by different anomalies in simulated anomaly images of the MVTec (Hazelnut data from Bergmann et al. (2019)) and BTAD (wood surface data from Mishra et al. (2021)). In Figure 2 (a), two different types of anomalies with different sizes were simulated. The comparison revealed that the image reconstruction of SSIM-AE was affected by the types and sizes of anomalies. Occasionally, due to the powerful learning capabilities of the model, SSIM-AE can even accurately recover the abnormal patches as demonstrated in Figure 2 (b), despite that the intention of reconstruction is to infer what the patch should be like *without* anomaly. Such results are especially critical when the image contains anomalies of multiple sizes: since some anomalies may cover multiple patches, certain anomaly patches are surrounded by other patches with anomalies. It is also worth mentioning that the anomaly contamination problem cannot be resolved by simply eliminating abnormal samples in the training phase. Even if we can do that, it is still unpredictable what the reconstructive model would generate if the input patches contained defects, as no defective patches were provided as training samples in the training phase. In fact, no method currently fully addresses the anomaly contamination problem.

In this paper, we develop an effective and computationally inexpensive image-based anomaly detection method for real-time image monitoring. This approach is called “Anomaly detection through identifying suspected patches” (Ano-SuPs). It is a reconstruction-based deep learning method for anomaly detection from images, specifically aimed at resolving the anomaly contamination problem to achieve high anomaly detection accuracy. Specifically, this benefit is achieved by an original two-stage strategy.

- In the first stage, the possible anomaly patches are identified based on reconstructing them with randomly selected patches and the vision transformer model. In this stage, randomly selected patches, instead of neighboring patches, are selected for reconstruction to avoid recovering one abnormal patch using other abnormal patches nearby.

This practice avoids missing abnormal patches of large sizes. Besides, the utilization of the attention-based vision transformer model is critical and unique as well, as it enables the accurate reconstruction of each patch based on randomly selected and potentially remote patches compared with traditional CNN models. Based on the reconstruction, we identify the suspected patches where anomalies may occur.

- The possible anomaly patches identified in the first stage may still have errors, given the possibility of having anomaly patches in the reconstruction input. In the second stage, we re-evaluate the suspected patches by reconstructing them using the non-suspected patches. Based on the re-evaluation, we identify the actual anomaly patches from the suspected anomaly patches obtained in the first stage.

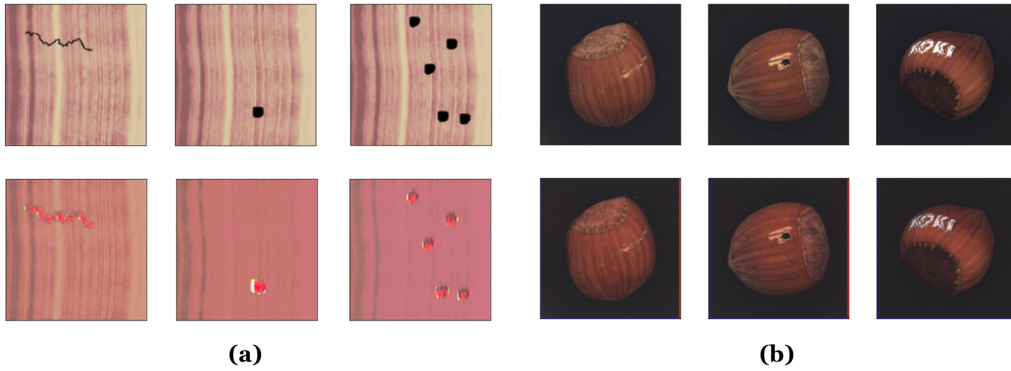


Figure 2: Two failed reconstruction cases by SSIM-AE (a) The first row shows the simulated images from BTAD wood surface data, and the second row shows the corresponding reconstructed images. (b) The first row shows the anomaly images from MVTEc Hazelnut data, and the second row shows the corresponding reconstructed images.

In the field of industrial image analysis, the proposed method makes the following contributions:

1. We identified a unique benefit of applying a vision transformer-based image reconstruction approach to an image-based anomaly detection problem: the Ano-SuPs approach demonstrates how the capability of image reconstruction based on random patches can contribute to defect identification of multiple sizes, and thus increases the robustness of the anomaly detection algorithms.

2. We devised a two-stage strategy that can mitigate the anomaly contamination problem to a large extent by identifying suspected anomaly patches in the first stage and eliminating them during the second reconstruction stage, to enable precise anomaly detection.

The rest of this paper is organized as follows. Section 2 reviews the related literature on the image-based anomaly detection field. Section 3 presents the proposed method. Section 4 provides the corresponding simulation experiments and a case study to evaluate the method’s performance. Further analysis of the proposed method to explore the factors that affect the model’s performance is also included. Finally, the conclusions of this paper are in Section 5.

2 Related work

This section provides a literature review of image-based anomaly detection in industrial applications. We first review the two categories of methods for image-based anomaly detection: additive matrix decomposition methods and deep learning methods. Then, we introduce the vision transformer, an important analytical tool that we utilize in the AnoSUPs method.

2.1 Additive matrix decomposition methods

In the field of industrial anomaly detection, the matrix decomposition method has been one of the mainstream approaches. The smooth sparse decomposition (SSD, Yan et al. (2017)), additive tensor decomposition (Mou et al. (2021)) and Robust Tensor Decomposition (Shen et al. (2022)) are the prominent examples. These methods assume that the normal region of the image is either smooth or low-rank, while the anomalies on the image are sparse regions. They use optimization problems to characterize the normal regions and the anomalous components. However, in real manufacturing applications, the assumption that the normal region of images is smooth or low-rank is very stringent, which significantly limits the application to the complex pattern and topography of a broader range of manufactured products. Besides, the additive matrix decomposition approaches typically

involve multiple tuning parameters to specify the trade-off between the requirement of background smoothness and anomaly sparsity, which presents another barrier to the effective and efficient implementation of the anomaly detection algorithm.

2.2 Deep Learning methods

Deep learning has become a dominant modeling approach nowadays in many machine learning applications due to its exceptional generalization capabilities and adeptness in handling high-dimensional data (Bergmann et al. (2022); Mou et al. (2023); Raghu et al. (2021); Pirnay and Chai (2022); Huang et al. (2021)). The techniques of using deep learning to perform image-based anomaly detection can be divided into two primary categories: representation-based approaches and reconstruction-based approaches. We review these approaches individually and discuss the studies that address the anomaly contamination problem.

- **Representation-based approaches.** The idea of representation-based approaches is first to establish the feature extraction function that maps the image samples into latent features and then perform the anomaly based on the discrepancy between the latent features of the current product and the population of latent features of normal products. One example is PaDiM (Defard et al. (2021)), which applies a pre-trained encoder to extract multi-scale features and describes the normal class as a mixture of Gaussian distributions, then performs anomaly detection by computing anomaly scores between the test feature and learned distribution. While in the manufacturing industry, there is a growing need for more precise anomaly information to be provided for downstream tasks such as root cause analysis. However, anomaly detection based on latent representations is lack of interpretability.
- **Reconstruction methods.** The workflow of reconstruction methods is first to establish a prediction function that reconstructs a patch of the image based on other parts of the image and then performs anomaly detection based on the reconstruction error of this patch. Reconstruction-based anomaly detection methods have the benefit of producing expected patches directly, which are commensurate with the patches of the original image and thereby lead to an intuitive understanding of the defects.

Along this line of research, the SSIM-AE (Bergmann et al. (2022)) method uses reconstruction error to guide anomaly segmentation, assuming the reconstructed error from the anomaly part will be larger. A Student-teacher network was further proposed in a study by Pirnay and Chai (2022), evaluating both predictive pixel uncertainties and regression error when comparing the output of the student network with that of a pre-trained teacher network trained on large natural images.

Only a few works have noticed the anomaly contamination issue in the introduction and attempted to address it formally using the learning algorithms (Mou et al. (2023); Dehaene et al. (2020)), yet none of them effectively solve the problem. For example, PAEDID (Mou et al. (2023)) addresses anomaly contamination through a carefully designed patch replacement scheme. They first employ an auto-encoder to train a patch generator based on images without anomalies and build a memory bank of their latent representations. They utilize the memory bank to perform anomaly detection of a new image by first replacing the suspected abnormal patch with an image generated from the memory bank with the closest representation and then solving an optimization problem to extract the anomalies. The motivation of the unique procedure is to use the crude background generated from the reconstruction model to guide the solution of the optimization problem and thereby locate the anomalies precisely. However, the memory bank, the search for the closest representation, and the solution of the optimization problem all add to the heavy space and time burden of computing. More critically, this practice is not robust against multi-size anomalies when large-sized anomalies are across multiple patches. Around large-sized anomalies, the neighbors of a normal patch may be abnormal and thereby have distinct representations from any representations of normal images in the memory bank, affecting the reconstruction of this normal patch and thus providing a false hint to the optimization problem.

2.3 Vision Transformers

In this paper, we develop a reconstructive approach that eliminates the effect of anomaly. The discussion from the introduction shows the necessity of reconstructing a patch in an image by using patches distributed across the entire image instead of the target patch's

neighbors. This goal is explicitly achieved by the Vision Transformer (ViT) model (Dosovitskiy et al. (2021)) using the masked mechanism proposed in He et al. (2022).

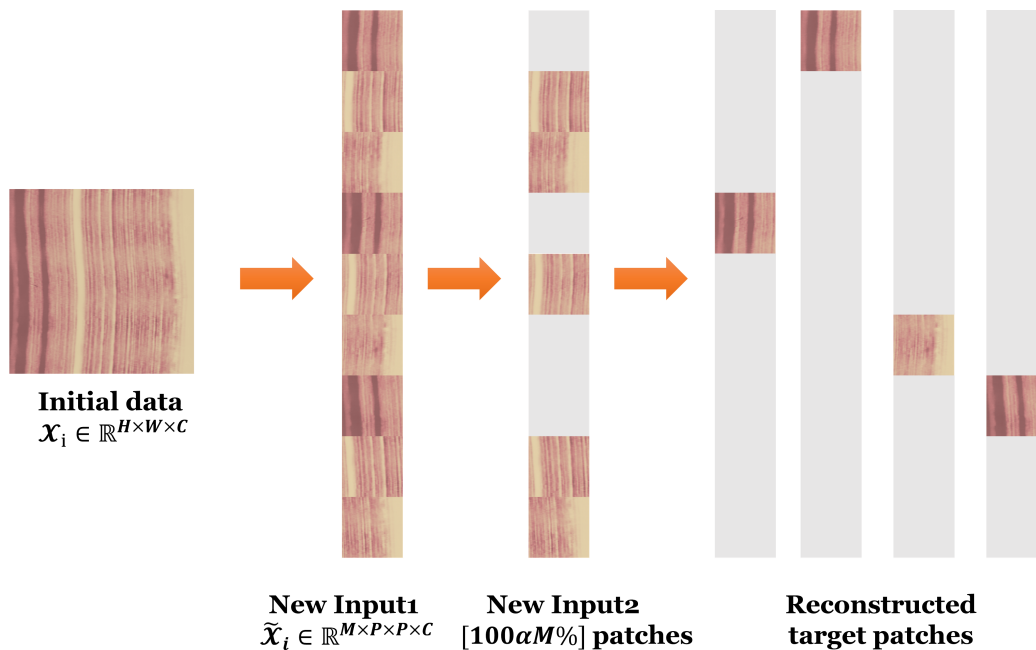


Figure 3: An illustration in the information processing of the ViT model using the masked mechanism. The masked patches are filled with zeros.

Due to the specific goal of patch reconstruction, the ViT model is trained with a specific configuration of input and output data. Suppose that we have N training images of size $H \times W$ with C channels, $\{\mathcal{X}_i \in \mathbb{R}^{H \times W \times C} : i = 1, \dots, N\}$ and suppose that each patch is a square of size $P \times P$ where $H \times W$ pixels can be divided into M square patches, i.e., $HW = MP^2$. Given the percentage of displaying patches α , the training samples of the ViT model are obtained with the following approach, as shown in Figure 3. First, an image \mathcal{X}_i is randomly selected from the training dataset and transformed into M patches $\tilde{\mathcal{X}}_i \in \mathbb{R}^{M \times P \times P \times C}$. From all M patches, $[100\alpha M\%]$ patches are randomly selected as observed patches, and another patch is selected as the target patch of reconstruction. The input data is $\tilde{\mathcal{X}}_i$ with all unobserved patches set to zeros, and the output is the target patch of reconstruction. The neural network architecture of ViT is designed for the input and output data described above and a transformer mechanism is applied therein to ensure a high accuracy rate of prediction based on relatively small α .

In the literature, few studies used vision transformers for anomaly detection in images. Among them, Mishra et al. (2021) used the Gaussian Mixture Model (GMM) to represent the latent vector of ViT, while the detailed anomaly detection approach is omitted, while Pirnay and Chai (2022) still reconstructed patches based on neighbors and calculated discrepancies so the anomaly contamination problem is not resolved. In conclusion, the ViT approach offers the possibility of developing a powerful anomaly detection approach, so our utilization of the ViT for this objective is original.

3 Proposed method

The overview of the proposed method is illustrated in Figure 4. Our Ano-SuPs approach is based on finetuning a pre-trained ViT network He et al. (2022) to obtain a patch reconstructor. Then we use a two-step procedure for anomaly detection as follows:

- Step 1** We randomly generate K incomplete images based on the image being tested, where each patch is randomly masked in one incomplete image and K is a tuning parameter of the method. Then, we reconstruct each patch by utilizing the unmasked patches of that incomplete image. We identify the *suspected patches with anomalies* based on the reconstruction error of this step.
- Step 2** We remove all suspected anomaly patches identified from Step 1 from the image being tested and generate an *incomplete image of normal patches*. Based on these normal patches, we reconstruct the suspected patches and compare the construction with the actual suspected patches, to decide whether they are real anomalies.

The underlying idea of the two-step procedure is described as follows. In Step 1, we use patches scattered on the entire image to reconstruct the image and thereby the reconstruction of anomaly patches will rely more on global information than on local information close to anomaly patches, resulting in a higher detection rate for anomaly patches. Nevertheless, a normal patch may still be recognized as an anomaly patch in Step 1, due to the possible anomalies in the patches that reconstruct this normal patch. Therefore, the type I error rate (normal patches being recognized as anomalies) is expected to be higher than the type II error rate (anomalies recognized as normal images), which indicates that the patches not

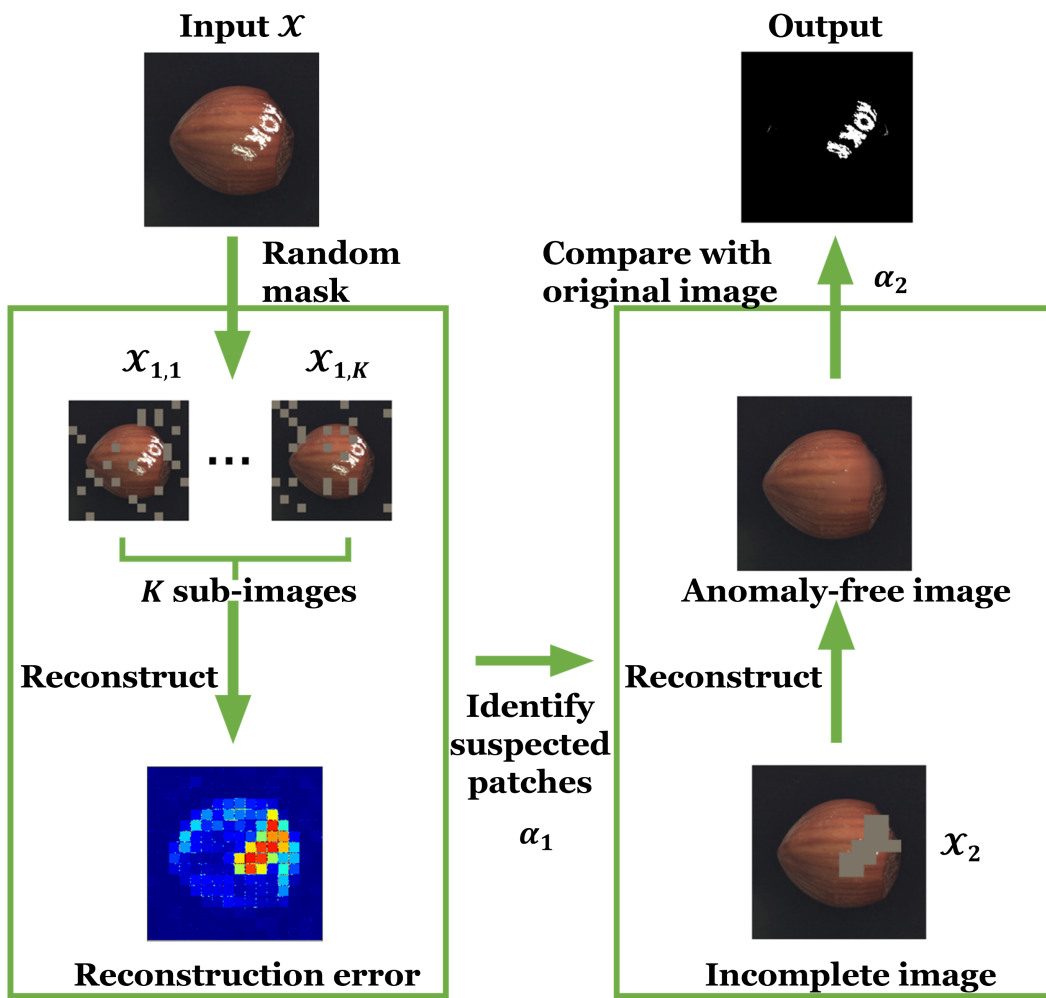


Figure 4: Overview of the proposed method

labeled as *suspected anomaly patches* are extremely likely to be normal. Since the input of Step 2 only contains the patches with no anomalies, the reconstruction accuracy for normal patches is further enhanced and thereby both type I and type II errors are improved after Step 2. In essence, Step 1 circumvents the anomaly contamination of Step 2.

Detailed descriptions of how we train the ViT model and how the two Steps are performed will be introduced in the remainder of this section and finally, we will provide several discussions of the model.

3.1 *Training patch reconstructor*

To prepare for our Ano-SuPs algorithm, we first train a patch reconstruction model by fine-tuning a pre-trained MAE. This MAE architecture incorporates ViT and thus has the capability of predicting a patch in an image from a fraction of other patches and the pre-trained model is developed by the authors of that paper with ImageNet-1K. However, since ImageNet-1K mainly includes nature images, we propose to fine-tune the reconstructor using images acquired from the same source as the ones being tested.

The overall fine-tuning approach is based on the input and output data format of MAE. Suppose that we have a library of training images $\mathcal{D}^{\text{train}} = \{\mathcal{X}_i^{\text{train}} : i = 1, \dots, N\}$ used for model fine-tuning. As illustrated in Figure 3, we generate each training sample of input and output as follows: we randomly pick one image $\mathcal{X}_i^{\text{train}}$ from the training image data set and transform it into patch representation $\tilde{\mathcal{X}}_i^{\text{train}} \in \mathbb{R}^{N \times P \times P \times C}$. We generate the input and output as introduced in the masking scheme of Section 2.3 with $\alpha = 1 - 1/K$. These pairs of input and output are fed into the optimizer to update MAE model parameters using the stochastic gradient descent method.

After the model is trained, we record the reconstruction error of all patches from the testing image. The empirical distribution of these errors will be used to specify the decision boundary of anomaly detection in the following Steps 1 and 2.

3.2 *Step 1: Identify suspected patches*

From the test image \mathcal{X} , we number all patches $i = 1, \dots, M$ based on their locations and divide them randomly and evenly into K groups of patches. Then we generate K incomplete images $\mathcal{X}_{1,k}, k = 1, \dots, K$, wherein all patches labeled within group k are removed from the

image k , $k = 1, \dots, K$. The subscript 1 denotes the incomplete images constructed in Step 1. As a result, all generated incomplete images have approximately $100(1 - 1/K)\%$ patches being masked, while all the masked patches reconstruct a complete image. An example with $K = 4$ incomplete images is shown in Figure 5.

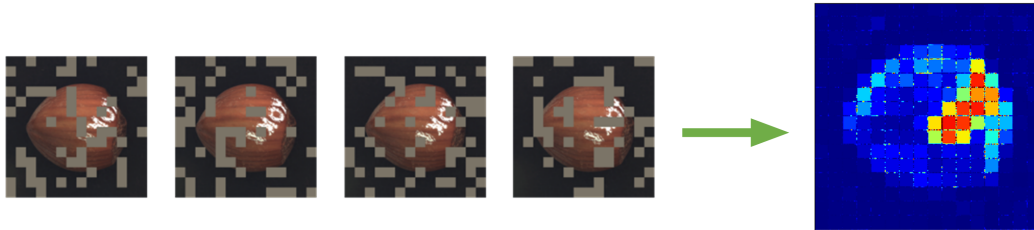


Figure 5: An example with $K = 4$ and the reconstruction error of Step 1

For each patch i of the original image $i = 1, \dots, M$, we identify the generated incomplete image $\mathcal{X}_{1,k(i)}$, where $k(i)$ is the index of the incomplete image within which the patch i is missing. Then we reconstruct the missing patch i within $\mathcal{X}_{1,k(i)}$ using the patch reconstructor obtained from Section 3.1 and the reconstructed patch is represented as $\hat{\mathcal{X}}_{1,k(i),i}$. We compare it with the actual patch in the original image $\tilde{\mathcal{X}}_i$ to calculate the reconstruction error

$$E_{1,i} = \left\| \hat{\mathcal{X}}_{1,k(i),i} - \tilde{\mathcal{X}}_i \right\|_F.$$

Finally, we compare each $E_{1,i}$ with q_{α_1} , the upper- α_1 sample quantile of the reconstruction error from the testing dataset and determine that a patch i is a *suspected patch with anomalies* if $E_{1,i} > q_{\alpha_1}$. The output of Step 1 is the set of all suspected patches, given as

$$\mathcal{S} = \{i : E_{1,i} > q_{\alpha_1}\}.$$

3.3 Step 2: Obtain anomaly results

After Step 1, we identified the set of suspected patches \mathcal{S} . As discussed at the beginning of this section, the patches with anomalies are only likely to appear in \mathcal{S} . Therefore, we generate another incomplete image \mathcal{X}_2 , where all patches in \mathcal{S} are missing. We then use the same patch reconstructor on individual patch $i \in \mathcal{S}$ and obtain the reconstructed patch $\hat{\mathcal{X}}_{2,i}$. Based on these reconstructed patches, we can calculate the reconstruction errors

$$E_{2,i} = \left\| \hat{\mathcal{X}}_{2,i} - \tilde{\mathcal{X}}_i \right\|, i \in \mathcal{S}.$$

The patches with $E_{2,i} > q_{\alpha_2}$ are decided as containing anomalies.

3.4 Discussions

The selection of tuning parameters. There are tuning parameters K , α_1 and α_2 . We postpone the discussion on selecting tuning parameters K and the SuPs step in the experiments. The tuning parameters α_1 and α_2 control the type I error of selecting suspected anomalies and making the final decision on the patches with anomalies: under the condition that all input patches of the reconstruction model do not have abnormal patches, α_1 and α_2 approximate the probability that a normal patch is recognized as a suspected patch or a anomaly. Therefore, we suggest choosing both α_1 and α_2 to be small as long as the patches with anomalies can be identified correctly.

Scope of applicability. The detailed description of Ano-SuPs indicates the scope of applicability of our method. In short, Ano-SuPs applies to regional anomalies with multiple sizes, where the total area of the anomalies is significantly smaller than the area of the normal regions. In Step 1, the anomaly patches in the inputs are inevitable, as long as the image contains anomalies. The limit of the area of anomaly indicates that the anomaly patches only appear in a small portion of all patches, ensuring that not many patches are influenced by the anomaly contamination problem in Step 1. In this way, abnormal patches can be recognized from their reconstruction (i.e., how the patch *should* look like) and be removed from Step 2.

Compared with our scope of applicability, the traditional image-based anomaly detection approaches typically require that the patch size and the defect size be compatible. Ano-SuPs alleviates this constraint and is capable of detecting multiple anomalies of different sizes.

Finally, we illustrate two cases for which the Ano-SuPs approach is not applicable and generates failures. They are illustrated in Figure 6. Both cases contain a large area of anomalies that can be mistaken as being a normal part, which undermines the unsupervised anomaly detection procedure.

- Figure 6 (a) displays an abnormal sample of a magnetic tile with uneven material distribution in the upper and lower parts of the tile. The anomaly type cannot be

detected by our method, because the anomaly is due to the large-scale uneven texture within the image.

- Figure 6 (b) displays a sample for an abnormal transistor whose mounting position does not meet the manufacturing standards. Detection of this anomaly requires specific semantic information and thereby is not distinguishable using our method.



Figure 6: Some samples that do not satisfy the anomaly assumption based on the proposed method

Insights on Ano-SuPs’ advantage. Besides the scope of applicability, the details of our method also bring insights into how the advantages of our reconstruction method are achieved.

1. **ViT leads to the effectiveness of screening in Step 1.** When reconstructing the patches in Step 1 based on input patches, the reconstruction of anomaly patches can use the information from other patches potentially far away based on the ViT architecture. For those normal image input patches, the reconstruction error of anomaly will be more noticeable.
2. **The screening leads to the effectiveness of anomaly identification of Step 2.** When we reconstruct the anomaly-free image after stage 1, there is no anomaly input in the reconstruction of the second stage, which effectively avoids the influence of anomaly in the reconstruction.
3. **Computational Efficiency.** Once the patch reconstructor is trained, our method only adds one more reconstruction step above the existing patch reconstruction, which

does not increase much computational burden. Besides, all K patch reconstruction operations in Stage 1 can be processed in parallel.

4 Experiments

In this section, three experiments are designed to test the performance of Ano-SuPs. Experiments 1 and 2 are based on two BTAD datasets (Mishra et al. (2021)) and Experiment 3 is based on MVTec datasets (Bergmann et al. (2019)), where the image size of three experiments is 224×224 . In all three experiments, we selected $K = 2$. Each image is divided into 196 small patches and the size of each patch is 16×16 . The products without defects in the BTAD dataset and the images generated by the simulation are illustrated in Figure 7. We generate and identify three types of anomalies that are common in manufacturing applications: cracks, colored regions and holes of different sizes. Specific configurations of the three anomaly types are as follows:

1. Line anomalies consist of irregular lines of defined length generated by random positions.
2. Color anomalies are fixed areas of random colors that appear in the original image.
3. Hole anomalies refer to a missing (i.e. black) region in the image. Hole type of anomaly has an indeterminate number but a fixed size and color.

Experiment 3 is based on the images in the MVTec hazelnut dataset, which comprises four types of anomalies within the images originally: Cut, Crack, Print and Hole. all these anomalies have different patterns as well as indeterminate sizes.

The study of related parameter K is conducted in an ablation study based on experiment 3 in Section 4.3.1. In all three experiments, the decision threshold is selected as the largest reconstruction error of the testing data obtained during the reconstruction model training phase. It corresponds to selecting α_1 and α_2 as a very small positive number.

Evaluation Criteria. We use the DICE to evaluate the performance of image-based anomaly detection (Zou et al. (2004)). This index is commonly used for assessing the performance of image segmentation and the problem of anomaly detection can be naturally

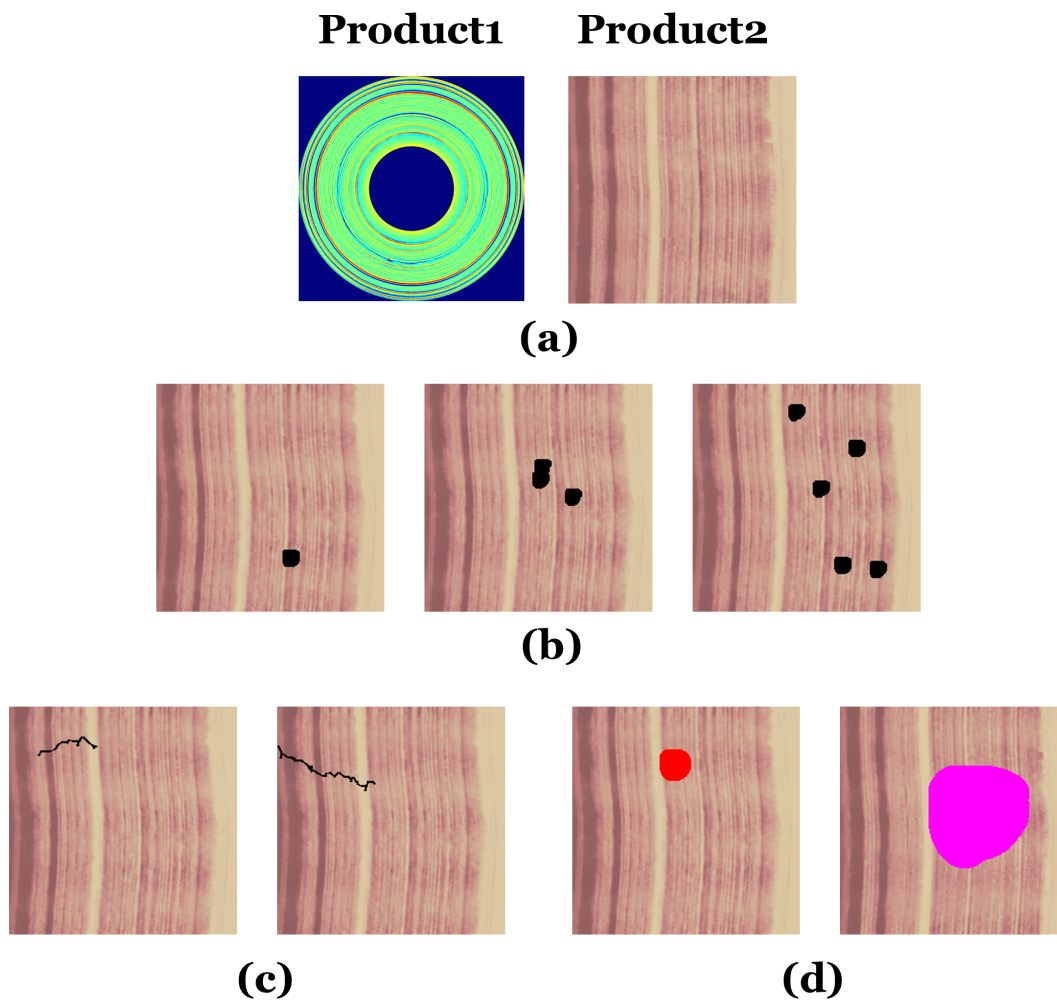


Figure 7: (a) Two products used in the BTAD dataset. (b) Simulated hole anomaly with varying numbers. (c) Simulated line anomaly with different lengths. (d) Simulated color anomaly with different sizes and random colors.

described as segmenting the anomaly region from the normal region of the image. Let A and B be the predicted and the actual defective region, the DICE index is defined as:

$$DICE(A, B) = \frac{2 \cdot \text{Area}(A \cap B)}{\text{Area}(A) + \text{Area}(B)} \in [0, 1],$$

and this index is consistent with the $F1$ score in binary classification problems. A larger DICE indicates better performance of the detection algorithm.

Methods of comparison. We compare Ano-SuPs with SSIM-AE and PAEDID. Among them the training of the SSIM-AE is based on the VGG structure (Simonyan and Zisserman (2015)) and the corresponding threshold value is obtained through cross-validation. The PAEDID method is selected as it also reconstructs an intermediate image to address the anomaly contamination problem. The neural network architecture of PAEDID is described in (Mou et al. (2021)), and we performed the parameter selection, including the predetermined percentile value (PPV) in the same way as the reference.

4.1 Experiment 1: The disk-shaped images in BTAD dataset

The results of anomaly detection for experiment 1 are summarized in Table 1. The average DICE for multi-size anomalies of the disk-shaped images is listed, and the standard deviation of the DICE scores for all generated anomalies of various sizes are reported inside the parentheses. As a reference of the anomaly detection capability, To understand the Ano-SuPs approach, the corresponding incomplete images after Step 1 are shown in Figure 8 (a), and the final reconstructed images and detected hole anomalies using all compared methods are illustrated in Figure 8 (b).

Table 1: Average DICE and standard deviation for Experiment 1

Type	Model		
	SSIM-AE	PAEDID	Ano-SuPs
line	6.68% (2.32%)	72.66% (0.17%)	86.39% (1.72%)
color	63.73% (3.62%)	92.14% (2.16%)	95.4% (0.02%)
hole	54.79% (18.42%)	91.93% (0.54%)	94.02% (0.18%)

For SSIM-AE, the model performance differs significantly with the types and sizes of anomalies being detected. For line anomalies, the DICE is only around 6% on average, but

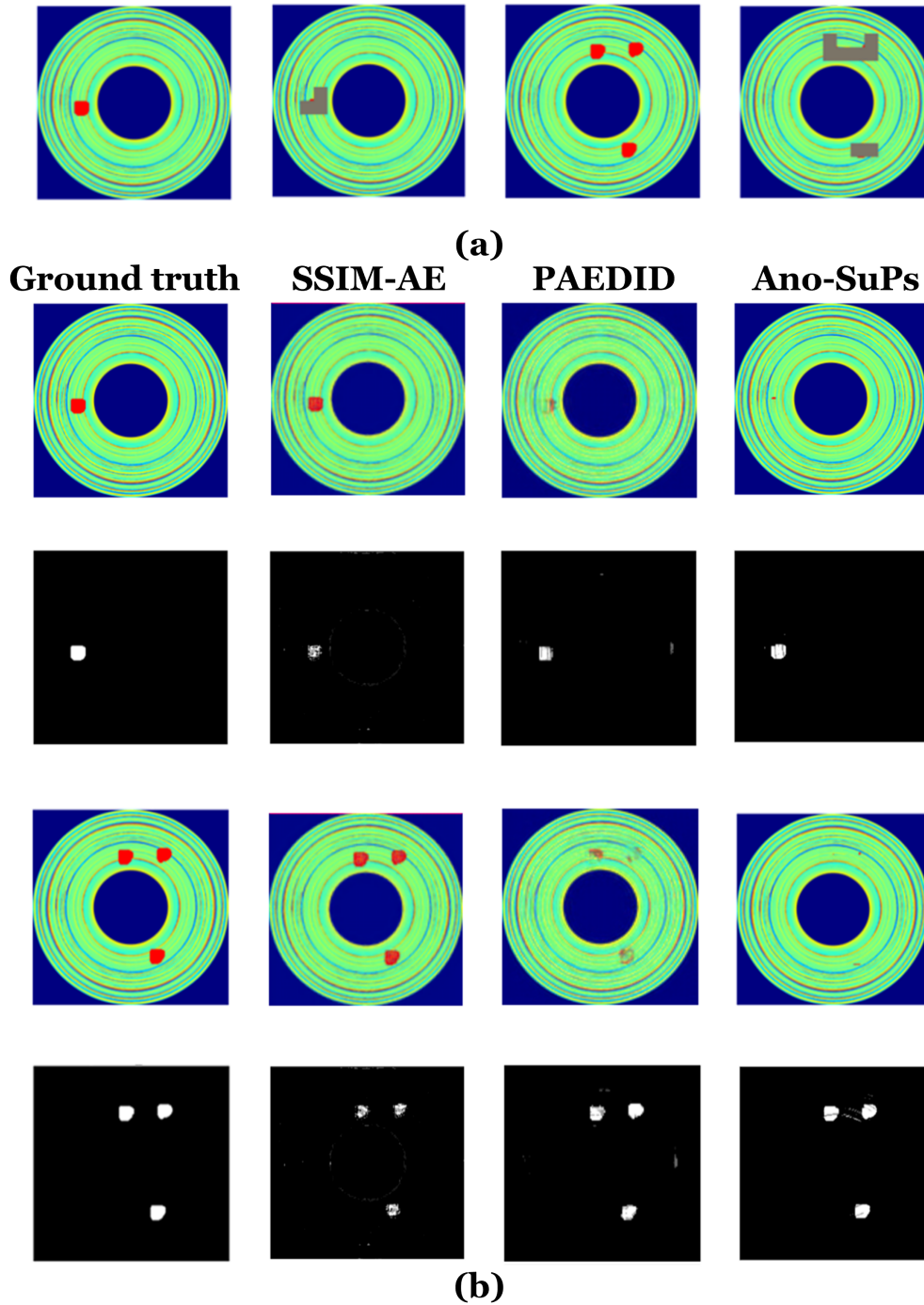


Figure 8: (a) The two test images and the corresponding incomplete image of disk shapes. (b) Comparison between the performance of SSIM-AE, PAEDID and Ano-SuPs for multiple sizes anomaly in disk-shaped images. The first column corresponds to the test image and simulated defective region and the rest of the columns correspond to the reconstructed image.

for hole anomalies and color anomalies, the average DICE are above 50%. The dependence of the detection capability on different anomaly sizes can be seen from the standard deviations of the DICE scores. The standard deviation of the DICE for hole anomalies is as high as 18.42%, indicating that the size of the anomaly dramatically impacts the performance of SSIM-AE, due to the anomaly contamination effect, evidenced by the fact that SSIM-AE reconstructs the anomaly regions with certain accuracy (Figure 8) and thus leads to low reconstruction error and poor anomaly detection rate.

For PAEDID, the model performance is relatively better than SSIM-AE. The DICE for the line anomaly is 72.66%, while the hole type and color type are above 90%. The prediction performance is also more stable for different anomaly sizes and the anomaly contamination problem is not significant with a proper PPV, as the reconstructed image contains few anomalies, which confirms the author’s conclusions. However, there are still traces of anomalies in the reconstructed image, indicating that the anomaly is not marked fully.

Our method has demonstrated superior performance in identifying diverse types of anomalies. The DICE for the line anomalies is 86.39% and the DICE for the hole or color anomalies is around 95%. The standard deviation of the DICE for different sizes of anomalies is also smaller compared to PAEDID and SSIM-AE. The standard deviation of the hole and color anomalies are both within 0.2%. The illustration of the suspected patches and the reconstructed image shows that all patches with anomalies are marked as suspected patches after Step 1 and the reconstructed image after Step 2 does not show any discernable anomalies.

4.2 Experiment 2: Wood surface images

The test results of the wood surface images are presented in Table 2 and Figure 9. In short, the overall findings confirm the result of Experiment 1.

For SSIM-AE, the DICE of the model varies considerably for different anomaly sizes, where the value for the color anomaly is the highest. The average DICE for line anomaly and hole anomaly is 28.64%. Observing the marked anomaly regions and the reconstructed images, the performance of the wood images is poorer than the disk-shaped images. Besides, even the normal part of the images is significantly modified by SSIM-AE. We suspect that

this is caused by the similarity between the wood texture (especially the stripes on the left side) and the morphology of the crack.

Table 2: Average DICE and standard deviation for Experiment 2

Type	Model		
	SSIM-AE	PAEDID	Ano-SuPs
line	28.64% (4.27%)	80.74% (3.38%)	99.83% (0.03%)
color	86.04% (6.3%)	93.44% (0.53%)	99.84% (0.03%)
hole	36.73% (15.97%)	94.96% (1.44%)	99.99% (0.02%)

The DICE for PAEDID achieves more than 90% for both color anomalies and hole anomalies. Also, the standard deviation of DICE is lower for PAEDID, indicating that the performance is more stable with various anomaly sizes. The reconstructed images in Figure 9 demonstrate that PAEDID does not introduce significant error but we can see the trace of a crack within the left-hand side of the image. This implies room for improvement in the anomaly identification of PAEDID, in terms of overcoming the anomaly contamination problem.

With our method, the DICE for the three types of anomalies are all greater than 99% and the standard deviations of these coefficients are all below 0.05%. Besides, our test process precisely recognizes the anomaly patch and reconstructs a high-quality anomaly-free image as shown in Figure 9, demonstrating our method’s reconstruction ability.

4.3 Experiment 3: Anomaly detection in hazelnut images

The corresponding results are shown in Table 3 and some examples of test images, reconstructed images and segmentation results of all models regarding print defect are exhibited in Figure 10. For SSIM-AE, due to the anomaly contamination problem, almost all patches with anomalies are identified, while the anomaly part has a relatively large reconstruction error, evidenced by the trace of anomalies in the reconstructed image in the first row.

PAEDID demonstrated a certain performance in this case study. Nonetheless, the reconstructed image reveals that the anomaly component remains present and the normal part has also been impacted, like the previous two examples. This is mainly due to the

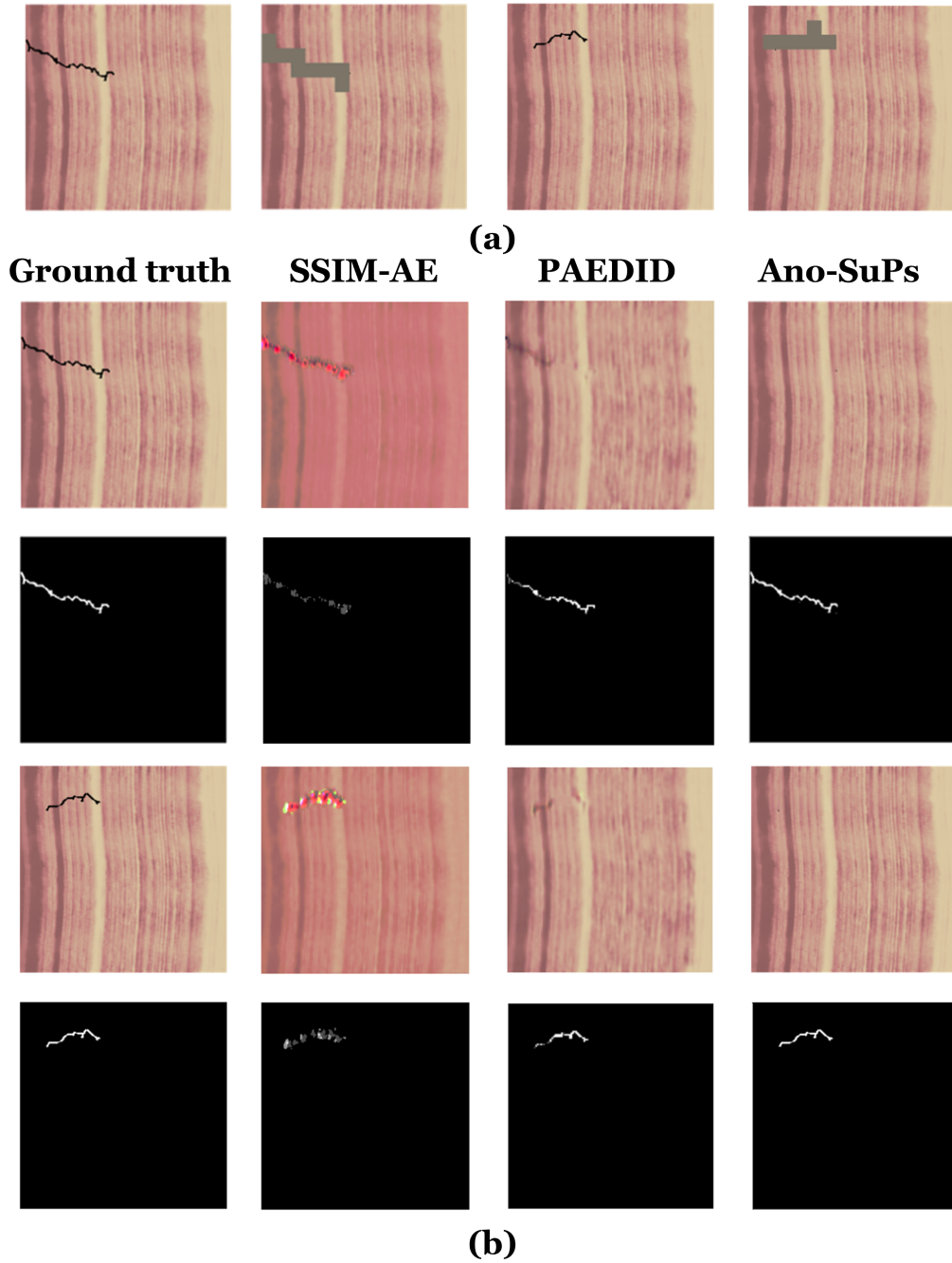


Figure 9: (a) The two test images and the corresponding incomplete image of wood surfaces. (b) Comparison between the performance of SSIM-AE, PAEDID and Ano-SuPs for multiple sizes anomaly in wood surface images. The first column corresponds to the test image and simulated defective region and the rest of the columns correspond to the reconstructed image.

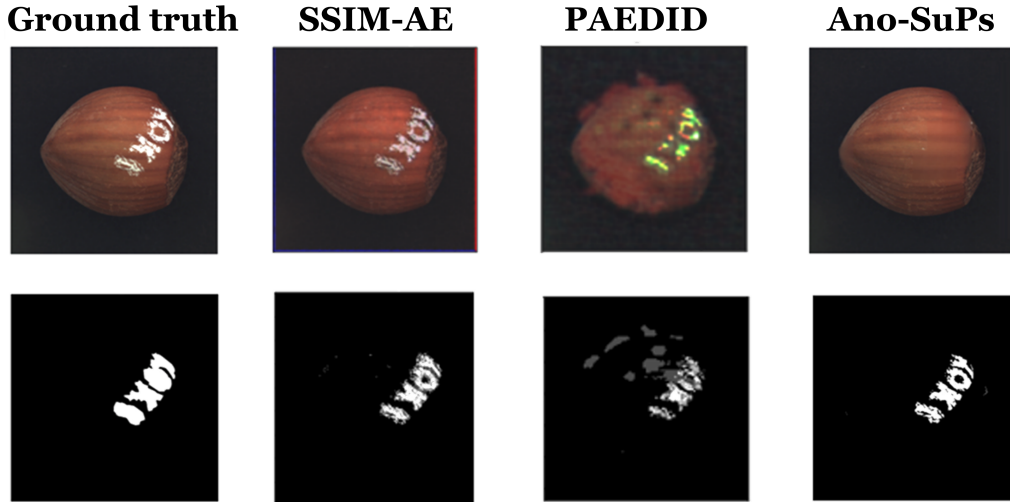


Figure 10: Comparison between the performance of SSIM-AE, PAEDID and Ano-SuPs for the “print” defect in the case study. The first row presents the test image and the reconstructed images for anomaly detection by the different methods, while the second row presents the ground truth defective region and the detected defective region obtained by the different methods.

Table 3: Average DICE in the Hazelnut case study

Type	Model		
	PAEDID	SSIM-AE	Ano-SuPs
Cut	14.07%	32.09%	46.68%
Crack	32.80%	28.77%	41.83%
Print	42.75%	67.75%	75.83%
Hole	22.21%	23.33%	60.90%

difficulty in selecting an appropriate decision threshold (the PPV value). The PPV value represents the proportion of anomalies replaced in the PAEDID model. In casestudy, since the size of anomalies is uncertain, it is difficult to match the PPV value with the real proportion of anomalies for each test sample. Too small a PPV value will result in incomplete removal of the anomaly, and too large a PPV value will result in too many replacements affecting the normal part. Additionally, the hazelnuts in the images have different positions

and orientations, which adds to the complexity of anomaly detection. These factors hinder the PAEDID’s performance in anomaly detection.

Our Ano-SuPs approach reaches the best results among the three methods for each anomaly type. It successfully identifies the anomaly patches and reconstructs an anomaly-free image, demonstrating its effectiveness in real-world anomaly detection scenarios. Although Step 1 of our method’s testing phase is the same as SSIM-AE and the reconstruction error for those anomalous patches is as large as the anomaly region we saw in SSIM-AE, Step 2 effectively avoids the anomaly contamination problem.

4.3.1 Ablation studies

To further investigate the impact of designed parameters on the model performance, we conducted an ablation study. Specifically, we focus on the selection of K and the comparison with the method that only uses Step 1 to perform anomaly detection using $E_{1,i}$ ’s directly. In this ablation study, we compare not only the performance index DICE but also the computational speed, which both factors are likely to affect. To account for the impact of random masks on the model, we conducted 10 repetitions of experiments and calculated both the mean and the standard deviation of the DICE. The results are illustrated in Table 4.

Our standard method achieves a 57.62% DICE for all anomalies with per image taking 1.81s.

Table 4: Average DICE and detection time of different factors

Model	Number of images	Time (s)	DICE	Standard deviation
One-step	2	1.16	45.04%	0.41%
Ano-SuPs	2	1.81	57.62%	0.47%
Ano-SuPs	4	2.99	57.13%	0.19%
Ano-SuPs	8	5.45	56.54%	0.28%
Ano-SuPs	16	11.14	56.34%	0.33%

In this table, the “One-step method” refers to the practice of performing anomaly detection directly based on the reconstruction error $E_{1,i}$ after Step 1. To evaluate the impact

of the Step 1. The One-step method yielded an average coefficient of 45.04% and required 1.16 s per image. For the standard deviation, the values for all the methods are below 0.5%, indicating that the random mask mechanism has an impact on the model performance. By contrast, when we apply the two-step procedure in Ano-SuPs, there is almost a 12% improvement in performance, albeit with a corresponding increase in computation times of approximately 0.6s. Our results underscore the importance of the two-step strategy in designing our method

For the parameter K , we systematically studied the results of using $K = 4, 8$ and 16 . Corresponding results show that the use of more patches yields a gradual decrease in the DICE from 57.62% to 56.34% and a significant increase in the testing time cost from 1.81s to 11.14s. As the number of K increases, an increasing portion of patches $(1 - 1/K)$ are involved in reconstructing the remaining patches. When the number of input patches increase, the reconstruction is increasingly dominated by the neighboring and abnormal patches within the inputs, thereby causing lower reconstruction error for anomaly patches in the first step due to the persisting anomaly contamination problem.

In summary, we verified that

- Both steps 1 and 2 are indispensable elements of the Ano-SuPs method that yield good performance. The SuPs step before anomaly detection has a huge impact on the model performance, yielding almost a 12% improvement.
- Varying from $K = 2$ to 16 leads to a gradual decrease of the DICE from 57.62% to 56.34% while a significant increase of testing time from 1.81s to 11.14s. Therefore, we suggest selecting $K = 2$ for a better trade-off between performance and computational time.

5 Conclusion

Image-based anomaly detection is a promising research topic in the manufacturing field. However, challenges such as variability and complexity of image background and multi-size anomaly hinder the application in manufacturing scenarios. The anomaly contamination problem we raised shows a research gap between existing methods and the existing image-based anomaly detection research.

In this article, we propose a two-stage Ano-SuPs approach to address the above problems and challenges. Our proposed method makes full use of the structural features of ViT, and the designed reconstruction of patches does not rely on the neighboring patches, ensuring the determination of multi-size anomalies. The two-stage strategy avoids the input of anomalies in the reconstruction process, addressing the anomaly contamination problem. Designed simulation experiments, as well as case studies, demonstrate the superiority of our approach and confirm the above conclusions. The influence of the parameters as well as the designed steps, is also addressed.

Notes on contributors

Hao Xu is an MPhil student from the Smart Manufacturing Thrust, Systems Hub, The Hong Kong University of Science and Technology (Guangzhou). He received his bachelor's degree in Materials Processing from Chongqing University in 2020 and his MSc degree in Data Science from City University of Hong Kong in 2022. His research focuses on anomaly detection in the manufacturing industry utilizing weakly supervised and unsupervised learning.

Juan Du is currently an assistant professor with the Smart Manufacturing Thrust, Systems Hub, The Hong Kong University of Science and Technology (Guangzhou), China. She is also affiliated with the Department of Mechanical and Aerospace Engineering, The Hong Kong University of Science and Technology, Hong Kong SAR, China and Guangzhou HKUST Fok Ying Tung Research Institute, Guangzhou, China. Her research interests include data analytics and machine learning for modeling, monitoring, control, diagnosis and optimization in intelligent manufacturing systems.

Andi Wang received a BS in statistics from Peking University in 2012, a Ph.D. in industrial engineering from Hong Kong University of Science and Technology in 2016, an MS in computer science and engineering from Georgia Institute of Technology in 2021 and a Ph.D. in Industrial Engineering from Georgia Institute of Technology in 2021. He is now an assistant professor at the Ira A. Fulton Schools of Engineering, Arizona State University. His research interests include smart manufacturing, data fusion and data-driven systems modeling, process monitoring and root cause diagnostics. He is a member of the Institute

of Industrial and Systems Engineers (IISE) and the Institute for Operations Research and the Management Sciences (INFORMS).

Acknowledgements

The authors acknowledge the generous support from the funding:

- Guangdong Basic and Applied Basic Research Foundation under Grant No.2023A1515-011656.
- National Natural Science Foundation of China under Grant 72001139.
- Guangzhou-HKUST(GZ) Joint Funding Program under Grant No.2023A03J0651.
- Guangzhou Municipal Science and Technology Program under Grant No.2022010-11235.

Related Resources Availability Statement

The pre-trained model is available at https://dl.fbaipublicfiles.com/mae/pretrain/mae_pretrain_vit_large.pth. MVTEC dataset is available at <https://www.mvtec.com/company/research/datasets/mvtec-ad>. BTAD dataset is available at <https://github.com/pankajmishra000/VT-ADL>.

References

- Behera, B. (2004). Image-processing in textiles. *Textile Progress* 35(2-4), 1–193.
- Bergmann, P., M. Fauser, D. Sattlegger, and C. Steger (2019). Mvtec ad—a comprehensive real-world dataset for unsupervised anomaly detection. In *Proceedings of the IEEE/CVF conference on computer vision and pattern recognition*, pp. 9592–9600.
- Bergmann, P., S. Löwe, M. Fauser, D. Sattlegger, and C. Steger (2022). Improving unsupervised defect segmentation by applying structural similarity to autoencoders. In *Proceedings of the 14th International Joint Conference on Computer Vision, Imaging and Computer Graphics Theory and Applications (VISIGRAPP)*, Volume 5, pp. 372–380.
- Defard, T., A. Setkov, A. Loesch, and R. Audigier (2021). Padim: a patch distribution modeling framework for anomaly detection and localization. In *Pattern Recognition. ICPR International Workshops and Challenges: Virtual Event, January 10–15, 2021, Proceedings, Part IV*, pp. 475–489. Springer.

- Dehaene, D., O. Frigo, S. Combrexelle, and P. Eline (2020). Iterative energy-based projection on a normal data manifold for anomaly localization. In *8th International Conference on Learning Representations, ICLR 2020, Addis Ababa, Ethiopia, April 26-30, 2020*. OpenReview.net.
- Dosovitskiy, A., L. Beyer, A. Kolesnikov, D. Weissenborn, X. Zhai, T. Unterthiner, M. Dehghani, M. Minderer, G. Heigold, S. Gelly, J. Uszkoreit, and N. Houlsby (2021). An image is worth 16x16 words: Transformers for image recognition at scale. In *9th International Conference on Learning Representations, ICLR 2021, Virtual Event, Austria, May 3-7, 2021*. OpenReview.net.
- Du, J., H. Yan, T.-S. Chang, and J. Shi (2021, 10). A Tensor Voting-Based Surface Anomaly Classification Approach by Using 3D Point Cloud Data. *Journal of Manufacturing Science and Engineering* 144(5), 051005.
- Fang, X., K. Paynabar, and N. Gebraeel (2019). Image-based prognostics using penalized tensor regression. *Technometrics* 61(3), 369–384.
- He, K., X. Chen, S. Xie, Y. Li, P. Dollár, and R. Girshick (2022). Masked autoencoders are scalable vision learners. In *Proceedings of the IEEE/CVF Conference on Computer Vision and Pattern Recognition*, pp. 16000–16009.
- Huang, F., B.-w. Wang, Q.-p. Li, and J. Zou (2021). Texture surface defect detection of plastic relays with an enhanced feature pyramid network. *Journal of Intelligent Manufacturing* 34, 1–17.
- Mishra, P., R. Verk, D. Fornasier, C. Piciarelli, and G. L. Foresti (2021). Vt-adl: A vision transformer network for image anomaly detection and localization. In *2021 IEEE 30th International Symposium on Industrial Electronics (ISIE)*, pp. 01–06. IEEE.
- Mou, S., M. Cao, H. Bai, P. Huang, J. Shi, and J. Shan (2023). Paedid: Patch autoencoder-based deep image decomposition for pixel-level defective region segmentation. *IJSE Transactions* 0(0), 1–15.
- Mou, S., A. Wang, C. Zhang, and J. Shi (2021). Additive tensor decomposition considering structural data information. *IEEE Transactions on Automation Science and Engineering* 19(4), 2904–2917.
- Pirnay, J. and K. Chai (2022). Inpainting transformer for anomaly detection. In *Image Analysis and Processing–ICIAP 2022: 21st International Conference, Lecce, Italy, May 23–27, 2022, Proceedings, Part II*, pp. 394–406. Springer.
- Raghu, M., T. Unterthiner, S. Kornblith, C. Zhang, and A. Dosovitskiy (2021). Do vision transformers see like convolutional neural networks? *Advances in Neural Information Processing Systems* 34, 12116–12128.
- Shen, B., R. R. Kamath, H. Choo, and Z. Kong (2022). Robust tensor decomposition based background/foreground separation in noisy videos and its applications in additive manufacturing. *IEEE Transactions on Automation Science and Engineering* 20(1), 583–596.

- Shi, J. (2023). In-process quality improvement: Concepts, methodologies, and applications. *IISE transactions* 55(1), 2–21.
- Simonyan, K. and A. Zisserman (2015). Very deep convolutional networks for large-scale image recognition. In Y. Bengio and Y. LeCun (Eds.), *3rd International Conference on Learning Representations, ICLR 2015, San Diego, CA, USA, May 7-9, 2015, Conference Track Proceedings*.
- Wang, K. and F. Tsung (2005). Using profile monitoring techniques for a data-rich environment with huge sample size. *Quality and reliability engineering international* 21(7), 677–688.
- Yan, H., K. Paynabar, and J. Shi (2017). Anomaly detection in images with smooth background via smooth-sparse decomposition. *Technometrics* 59(1), 102–114.
- Yan, H., K. Paynabar, and J. Shi (2018). Real-time monitoring of high-dimensional functional data streams via spatio-temporal smooth sparse decomposition. *Technometrics* 60(2), 181–197.
- Zou, K. H., S. K. Warfield, A. Bharatha, C. M. Tempany, M. R. Kaus, S. J. Haker, W. M. Wells III, F. A. Jolesz, and R. Kikinis (2004). Statistical validation of image segmentation quality based on a spatial overlap index1: scientific reports. *Academic radiology* 11(2), 178–189.